High-quality NbN nanofilms on a GaN/AlN heterostructure

Diane Sam-Giao, Stéphanie Pouget, Catherine Bougerol, Eva Monroy, Alexander Grimm, Salha Jebari, Max Hofheinz, J.-M. Gérard, and Val Zwiller

High-quality NbN nanofilms on a GaN/AlN heterostructure

Diane Sam-Giao,[1,2,3] Stéphanie Pouget,[1,2] Catherine Bougerol,[1,4]
Eva Monroy,[1,2] Alexander Grimm,[1,3] Salha Jebari,[1,3] Max Hofheinz,[1,3]
J.-M. Gérard,[1,2] and Val Zwiller[1,3,5]
[1]*Université Grenoble Alpes, 38000 Grenoble, France*
[2]*CEA-Grenoble, INAC/SP2M, 17 avenue des Martyrs, 38054 Grenoble, France*
[3]*CEA-Grenoble, INAC/SPSMS, 17 avenue des Martyrs, 38054 Grenoble, France*
[4]*Institut Néel-CNRS, 25 avenue des Martyrs, 38042 Grenoble, France*
[5]*Kavli Institute of Nanoscience, Delft University of Technology, 2628 CJ Delft,
The Netherlands*

We demonstrate high-quality monocrystalline NbN films deposited by DC magnetron sputtering on a GaN/AlN waveguiding heterostructure. NbN layers with a thickness of 8 nm are grown along the [111] direction, and show two orientation domains with NbN(111) [2-1-1]//AlN (0001) [10-10] and NbN(111) [2-1-1]//AlN(0001) [01-10] epitaxial relationships. Our NbN films display a critical temperature of 13.2 K, with the superconducting transition taking place in a temperature range of only 0.7 K. *© 2014 Author(s). All article content, except where otherwise noted, is licensed under a Creative Commons Attribution 3.0 Unported License.* [http://dx.doi.org/10.1063/1.4898327]

Quantum optics is undergoing tremendous progress, both conceptually and experimentally. An important remaining challenge is single-photon detection with near-unity efficiency, high time resolution, low dark counts and photon-number resolution. Detection is usually carried out using semiconductor-based avalanche photodiodes; however, this technology is limited by large timing jitter, unavoidable dark counts, after pulsing, and limited detection efficiency.[1] A new paradigm in nanophotonics was introduced in 2001 when single-photon detection was demonstrated with superconducting nanowire single-photon detectors (SNSPDs).[2] When a photon is absorbed by a superconducting nanowire biased just below its critical current, it triggers a transition from the superconducting to the normal state, resulting in a voltage spike at the nanowire leads. Superconductivity is then recovered within a few nanoseconds. Over the past decade, large progress has been made with this technique.[3,4] The detection efficiency can be increased by coupling the superconducting nanowire to the evanescent field propagating in a waveguide. SNSPDs consisting of NbN-based nanowires Si_3N_4 waveguides have led to 80% on-chip detection efficiency at 768 nm,[5] and Si waveguides have allowed record 91% on-chip detection efficiency at telecom wavelengths.[6] However, the fabrication of high quality, ultra-thin, superconducting layers on top of such materials is challenging. NbN films with a thickness of 3-4 nm have been epitaxially grown on 3C-SiC, but they display stacking faults and twinning defects originating from the SiC substrate, which resulted in a critical temperature of only 11.8 K,[7] to be compared to 16 K for thick NbN films.[8,9] Various buffer layers have been tested to achieve the growth of high-quality ultra-thin (5-10 nm) NbN layers, but they all proved to be polycrystalline and displayed a critical temperature between 8.3 and 13 K.[7]

GaN/AlN semiconductors, with a transparent band from 400 to 6000 nm, their mechanical and thermal robustness and the maturity of their technology, appear as a promising material system for waveguide fabrication.[10] Furthermore, the strong electro-optic effects in III-nitrides open the possibility of on-chip polarization control. It has been demonstrated that III-N substrates yield improved NbN layer properties (higher critical temperature and lower resistivity[11]) because of the relatively close lattice parameters of cubic NbN (111) and wurtzite GaN or AlN (0001) (2.1% lattice mismatch with GaN and <0.2% with AlN). In this sense, NbN nanofilms on GaN buffers grown by metalorganic vapor phase epitaxy (MOVPE) on sapphire substrates with a superconducting critical

temperature of 13.2 K (measured at 50% of the resistance drop) and a transition width $\Delta T = 1.1$ K have been recently reported.[12]

In this work, we present high-quality NbN films on a (0001)-oriented GaN/AlN heterostructure fabricated by plasma-assisted molecular-beam epitaxy (PAMBE). The NbN layers are (111)-textured and present domains characterized by two different epitaxial relationships: NbN(111) [2-1-1]//AlN (0001) [10-10] and NbN(111) [2-1-1]//AlN(0001) [01-10]. The superconducting transition takes place in a temperature range of only 0.7 K and extrapolates to zero resistance at 13.1 K.

Thin (~8 nm) NbN layers were deposited by DC magnetron sputtering on a GaN/AlN waveguiding heterostructure consisting of a 650-nm-thick GaN layer deposited by PAMBE on a 1.1-μm-thick AlN-on-sapphire template.[11] The GaN growth was performed at a growth rate of 300 nm/h, a substrate temperature of 720 °C, and under slightly Ga-rich conditions, i.e. with a self-regulated Ga film on the growth front.[13–15] NbN was deposited by DC magnetron sputtering at 4 A and 420 V, from a high purity 6" Nb target with Ar (partial pressure 1.67×10^{-2} mbar) and nitrogen (partial pressure 0.20×10^{-2} mbar) process gases, with the nitrogen gas partially nitridating the target surface. Prior to the deposition, the samples were heated to approximately 300 °C and cleaned with argon plasma. Total deposition time was 14 s during which the sample was swept several time over the target, with an effective time over the target of approximately 2 s.

Figure 1 compares the surface morphology of an NbN layer and that of the GaN/AlN waveguiding structure, both measured by atomic force microscopy operated in the tapping mode. The GaN surface presents monoatomic steps with the spiral patterns characteristic of III-nitride semiconductors grown by PAMBE.[13] The root-mean-square (rms) surface roughness is ~0.5 nm. In the case of the NbN layer, the GaN morphology is still distinguishable, but it appears covered by a thin grainy layer with an rms roughness of ~2.0 nm.

The crystalline structure of the layer was characterized using x-ray diffraction measurements (XRD) in a Panalytical Empyrean diffractometer equipped with a Cobalt anode beam tube (Co $\lambda_{K\alpha} = 1.789$ Å), a Göbel mirror and a two-dimensional pixel detector used in both zero-dimensional and one-dimensional modes. Figure 2 shows the θ-2θ diffractogram of an NbN/GaN/AlN sample, dominated by the reflection lines originating from the sapphire substrate and the comparatively thick GaN and AlN layers. The NbN (111) line is hardly discernible due to its high overlap with GaN (0002) and AlN (0002). For higher angles, and therefore higher Miller indices, the three contributions are more dispersed and a well-resolved NbN (222) reflection is observed at 2θ = 89.4°. The fact that only (*hhh*) type reflections from the NbN layer are detected shows that the layer is textured along the [111] direction.

To assess the mosaicity of the NbN layer, rocking curves have been measured around the NbN (222) reflection, as illustrated in the inset of Fig. 2. Two components are identified, a narrow peak attributed to the mosaicity inside the NbN domains, and a broader contribution associated to the lateral size of these domains. This measurement was repeated with different detector angular acceptances. Whereas the width of the narrow peak varies with the resolution, preventing us from
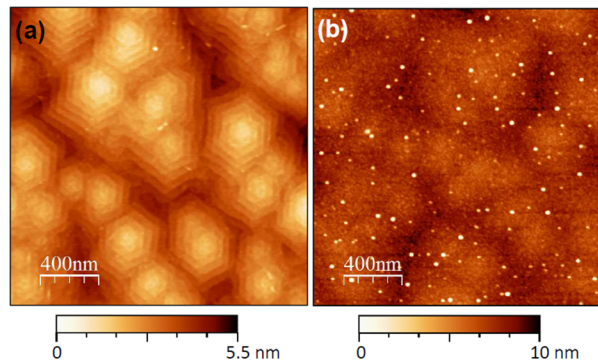
FIG. 1. Atomic force microscopy images of the surface of (a) the GaN layer prior to NbN deposition, and (b) an 8 nm thick NbN layer. Extracted rms roughness is 0.75 nm and 1.5 nm for images (a) and (b), respectively.
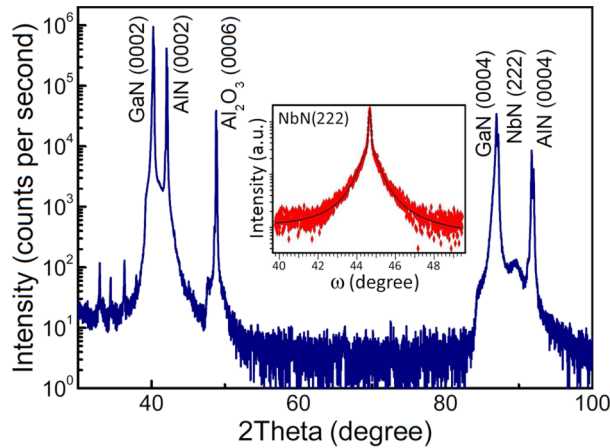
FIG. 2. XRD θ-2θ scan along the (111) and (222) NbN reflections. The NbN (111) reflection is not resolved due to the proximity of GaN (0002) and AlN(0002). Inset: Rocking curve around the NbN (222) reflection.

determining the mosaicity, the broader component remains constant with a full width at half maximum $\Delta\omega = 0.87°$. An average lateral size of the domains $L = 8\pm1$ nm can be deduced from this $\Delta\omega$ using the Scherrer formula:

$$L = \frac{\lambda}{2sin\theta\Delta\omega}$$

In order to get a deeper insight into the in-plane crystalline quality of the NbN layer, asymmetrical XRD reflections have been studied. The inset of Fig. 3 displays the result of an azimuthal scan performed for 2θ fixed at the (311) Bragg angle value $2\theta_B$ and the incident angle ω fixed at $\theta_B + \alpha$ where α is the angle between both [111] and [311] directions. The presence of equidistant peaks shows that the NbN layer is monocrystalline. However, for a cubic lattice with a [111] growing direction, we expect a three-fold symmetry, i.e. a 120° periodicity. The 60° periodicity displayed in the inset of Fig. 3 can be attributed to the coexistence of two orientations for the NbN, induced by the six-fold symmetry of the GaN/AlN waveguide.

Figure 3 depicts a reciprocal space map obtained around the NbN (311) and AlN and GaN (10-13) reflections. Considering that the in-plane ($Q^{//}$) and perpendicular ($Q^{\perp}$) components of
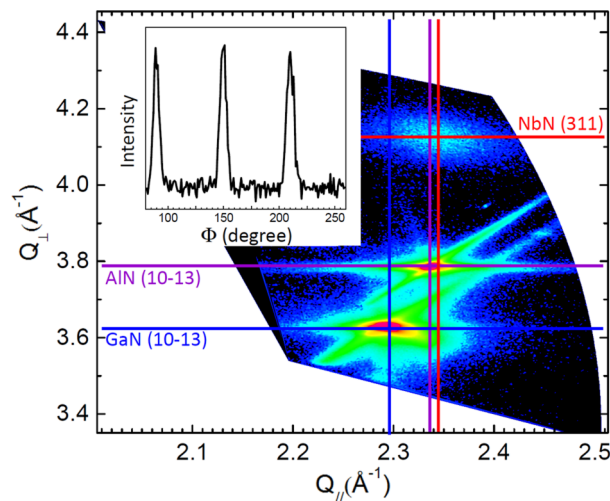
FIG. 3. Reciprocal space map at Φ=89.61° and the offset angle α = 29.5° displaying the NbN (311), AlN and GaN (10-13) reflections. Inset: Azimuthal scan for the NbN (311) reflection (2θ = 84.5529° and ω = 71.77645°).

the reciprocal space vectors associated to the NbN (311) reflection are $\vec{Q}_{(311)}^{//} = 2/3\,\vec{Q}_{(2\bar{1}\bar{1})}$ and $\vec{Q}_{(311)}^{\perp} = 5/3\vec{Q}_{(111)}$, the in-plane and perpendicular lattice parameters of each layer ($d_{[2\text{-}1\text{-}1]}$ and $d_{[111]}$ for NbN, and a and c for GaN and AlN) have been calculated from the positions of each line, with the results presented in Table I. The values of the NbN lattice parameter extracted from the measurement of $d_{[2\text{-}1\text{-}1]}$ or $d_{[111]}$ assuming a regular cubic lattice are also presented in the table ($a_{//}$ and $a_{\perp}$, respectively). The difference between the values of $a_{//}$ and $a_{\perp}$ points to a residual in-plane compressive strain of 0.3±0.1%.

The microstructure of the samples has been analyzed by high-resolution transmission electron microscopy. The samples were prepared in cross-section by mechanical polishing followed by ion milling. Figure 4(a) shows an image of the NbN layer on GaN, taken along the [11-20] zone axis of GaN. The NbN layer is about 8 nm thick. It is formed by the coalescence of islands (Volmer-Weber growth), all grown along the <111> NbN direction, which is aligned with the [0001] GaN axis. However, they have two distinct orientations, namely NbN(111) [2-1-1]//AlN (0001) [10-10] and NbN(111) [2-1-1]//AlN(0001) [01-10]. These orientations correspond to a 60° rotation of the lattice with respect to the growth axis, as identified by the fast-Fourier transform patterns presented in Figs. 4(b) and (c) together with a structural model describing the atomic arrangements. Such rotation domains are commonly observed when growing a cubic material along [111] on top of the (0001) plane of a hexagonal substrate. The presence of two crystallographic orientations explains the 60° periodicity observed by XRD (inset of Fig. 3). No periodic array of dislocations is visible at the GaN/NbN interface. This is likely due to the lateral extension of the islands which is smaller than the expected dislocations period, as well as their three dimensional nature which allows elastic relaxation.

In order to assess the electronic quality of the NbN layers, measurements of the critical temperature were performed by varying the temperature from 300 K to 4 K. Figure 5 displays the evolution of the resistance of an NbN layer as a function of temperature. The room-temperature resistance measured with a four-probe experiment was $R_{\square} = 220\ \Omega$. In the 14 – 300 K range, the resistance increases with decreasing temperature as expected for highly-resistive metallic layers, peaking at 248 Ω at 38 K. This behavior is consistent with the existence of grains whose joints decrease the electron mean free path when temperature decreases. The left panel shows the superconducting transition on a finer temperature scale. The critical temperature was extracted by extrapolating the resistance curve to zero:[16] we obtained a value of 13.1 K (13.2 K at 50% of the resistance drop), higher than the 10.5 K reported for NbN layer on sputtered AlN on silicon,[11] and identical to NbN on GaN buffers grown by MOVPE.[12] The resistance decreases abruptly over a narrow temperature range ΔT = 0.7 K, taken as the difference between the temperatures corresponding to a resistance drop of 10% and 90% from the maximum value. This rather sharp transition, smaller than the ΔT = 1.1 K reported on monocrystalline NbN nanofilms on 3C-SiC[7] and on MOVPE GaN buffers,[12] indicates the outstanding electronic properties of the layer.

TABLE I. Lattice parameters extracted from various XRD reflections. In the case of NbN, the lattice parameters along [2-1-1] and [111] are extracted from the XRD reflections, and $a_{//}$ and $a_{\perp}$ are the cubic lattice parameters calculated from $d_{[2\text{-}1\text{-}1]}$ or $d_{[111]}$ assuming a regular cubic lattice.

Material	Reflection	Lattice parameter
NbN	(311)	$d_{[2\text{-}1\text{-}1]} = 1.791 \pm 0.005$ Å ($a_{//} = 4.387$ Å)
		$d_{[111]} = 2.539 \pm 0.005$ Å ($a_{\perp} = 4.398$ Å)
	(222)	$d_{[111]} = 2.541 \pm 0.005$ Å ($a_{\perp} = 4.401$ Å)
GaN	(10-13)	$a = 3.170 \pm 0.005$ Å
		$c = 5.197 \pm 0.005$ Å
	(0004)	$c = 5.199 \pm 0.005$ Å
AlN	(10-13)	$a = 3.108 \pm 0.005$ Å
		$c = 4.983 \pm 0.005$ Å
	(0004)	$c = 4.984 \pm 0.005$ Å

FIG. 4. (a) High-resolution transmission electron microscopy image taken along the [11-20] zone axis of the GaN substrate showing that the NbN layer is formed by islands. (b),(c) fast-Fourier transform pattern and structural models of both islands marked by the squares in (a) and having a different orientations.
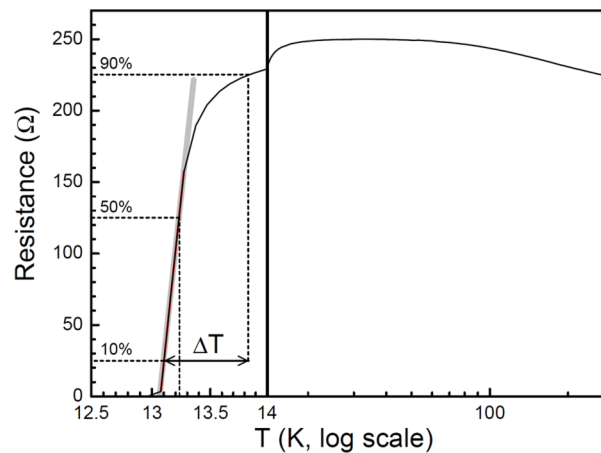
FIG. 5. Resistance of the NbN layer as a function of temperature. The grey line is a linear fit of R(log T) around the critical temperature. It extrapolates to zero resistance at 13.1 K (the critical temperature at 50% drop of the resistance is 13.2 K). The resistance decrease takes place over a rather narrow temperature range $\Delta T = 0.7$ K.

We have demonstrated the deposition of monocrystalline NbN (111) films on a (0001)-oriented GaN/AlN waveguide. NbN layers are quasi-relaxed through a Volmer-Weber growth mechanism. They are characterized by the coexistence of two epitaxial relationships with NbN(111) [2-1-1]//AlN (0001) [10-10] and NbN(111) [2-1-1]//AlN(0001) [01-10]. An 8-nm-thick NbN-on-GaN/AlN film displays a critical temperature of 13.1 K (13.2 K at 50% of the resistance drop). The superconducting transition takes place over a temperature range of only 0.7 K. This result enables the fabrication of high performance photonic circuits exploiting the electro-optic effects of III-nitrides.

ACKNOWLEDGMENTS

[1] R. H. Hadfield, Nature Photonics **3**, 696 (2009).

[2] G. N. Gol'Tsman, O. Okunev, G. Chulkova, A. Lipatov, A. Semenov, K. Smirnov, B. Voronov, A. Dzardanov, C. Williams, and R. Sobolewski, Appl. Phys. Lett. **79**, 705 (2001).

[3] S. N. Dorenbos, E. M. Reiger, U. Perinetti, V. Zwiller, T. Zijlstra, and T. M. Klapwijk, Appl. Phys. Lett. **93**, 131101 (2008).

[4] M. G. Tanner, C. M. Natarajan, V. K. Pottapenjara, J. A. O'Connor, R. J. Warburton, R. H. Hadfield, B. Baek, S. Nam, and S. N. Dorenbos, Appl. Phys. Lett. **96**, 221109 (2010).

[5] C. Schuck, W. H. P. Pernice, and H. X. Tang, Appl. Phys. Lett. **102**, 051101 (2013).

[6] W. H. P. Pernice, C. Schuck, O. Minaeva, M. Li, G. N. Goltsman, A. V. Sergienko, and H. X. Tang, Nature Communications **3**, 1325 (2012).

[7] J. R. Gao, M. Hajenius, F. D. Tichelaar, T. M. Klapwijk, B. Voronov, E. Grishin, G. Goltsman, C. A. Zorman, and M. Mehregany, Appl. Phys. Lett. **91**, 062504 (2007).

[8] T. H. Courtney, J. Reintjes, and J. Wulff, J. Appl. Phys. **36**, 660 (1965).

[9] C. M. Yen, L. E. Toth, Y. M. Shy, D. E. Anderson, and L. G. Rosner, J. Appl. Phys. **38**, 2268 (1967).

[10] L. Monteagudo-Lerma, S. Valdueza-Felip, F. B. Naranjo, P. Corredera, L. Rapenne, E. Sarigiannidou, G. Strasser, E. Monroy, and M. González-Herráez, Optics Express **21**, 27578 (2013).

[11] T. Shiino, S. Shiba, N. Sakai, T. Yamakura, L. Jiang, Y. Uzawa, H. Maezawa, and S. Yamamoto, Supercond. Sci. and Technol. **23**, 045004 (2010).

[12] S. Krause, D. Meledin, V. Desmaris, A. Pavolotsky, V. Belitsky, M. Rudzinski, and E. Pippel, Supercond. Sci. Technlol. **27**, 065009 (2014).

[13] B. Heying, R. Averbeck, L. F. Chen, E. Haus, H. Riechert, and J. S. Speck, J. Appl. Phys. **88**, 1855 (2000).

[14] C. Adelmann, J. Brault, G. Mula, B. Daudin, L. Lymperakis, and J. Neugebauer, Phys. Rev. B **67**, 165419 (2003).

[15] P. K. Kandaswamy, H. Machhadani, Y. Kotsar, S. Sakr, A. Das, M. Tchernycheva, L. Rapenne, E. Sarigiannidou, F. H. Julien, and E. Monroy, Appl. Phys. Lett. **96**, 141903 (2010).

[16] P. C. J. J. Coumou, E. F. C. Driessen, J. Bueno, C. Chapelier, and T. M. Klapwijk, Phys. Rev. B **88**, 180505 (2013).